CLIO report

Khodnevych Vitalii, Nicolas Delerue

June 20, 2017

1 Introduction

Smith-Purcell radiation (SPR) occurs when a charged particle move above a metallic periodic structure. Emitted radiation is spread in solid angle. The wavelength of the radiation for SPR depends on the observation angle Θ according to the following formula:

$$\lambda = \frac{l}{n}(\frac{1}{\beta} - cos\Theta) \tag{1}$$

where l is the grating period , n is the order of radiation, Θ is the observation angle and β is the relativistic velocity.

For one electron the emission spectrum (single electron yield [?]) is given by:

$$\frac{d^2 I_1}{d\omega d\Omega} = \frac{e^2 \omega^2 l^2}{4\pi^2 c^3} R^2 exp(-2x_0/\lambda_e) \tag{2}$$

where ω is the emission frequency, $d\Omega$ is the solid angle, e is the electron charge, c is the speed of light, R^2 is the "grating efficiency factor", x_0 is the beam-grating separation (BGS) and λ_e is the evanescent wavelength:

$$\lambda_e = \lambda \frac{\beta\gamma}{2\pi\sqrt{1 + (\beta\gamma \sin\Theta \sin\phi)^2}} \tag{3}$$

where β, γ are the relativistic parameters of the particles in the beam. The total spectrum is proportional to the single electron yield and contains incoherent and coherent components:

$$\frac{d^2 I}{d\omega d\Theta} = \frac{d^2 I_1}{d\omega d\Theta}[N + N(N-1)F(\omega)] \tag{4}$$

Where N is the number of electrons in the bunch and $F(\omega)$ is the form factor of the time profile of the bunch. Using the phase recovery methods, such as Kramers-Kronig or Hilbert [?], it is possible to recover the phase and then the time profile of the bunch.

So Smith-Purcell radiation can be used to monitor the longitudinal beam profile.

2   CLIO installation/Experimental setup

The experimental setup is shown on figure 1. It consist of 12 pyrodetectors placed from 48° to 125° with 7° separation. To collect the emitted radiation 25 mm diameter off-axis parabolic mirrors are used. The signal from the detectors is amplified and then digitized by a data 12 bits 1 MS/s acquisition system.

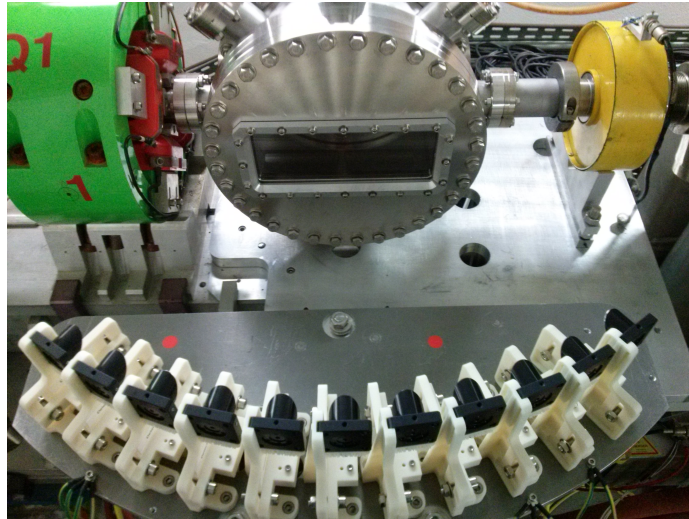The experiment uses a 40x20 mm aluminium grating with 3 mm pitch. The beam-grating separation can be changed by a stepper motor.

Figure 1: Experimental setup for SPR measurements at CLIO: set of twelve pyrodectors with off axis parabolic mirrors placed equidistantly with 7° separation and experimental chamber with the grating inside.

3   CLIO

The CLIO free electron laser is an accelerator built in 1991. It is described in details in [?] and it is shown on figure 2. The CLIO accelerator consist of a thermionic
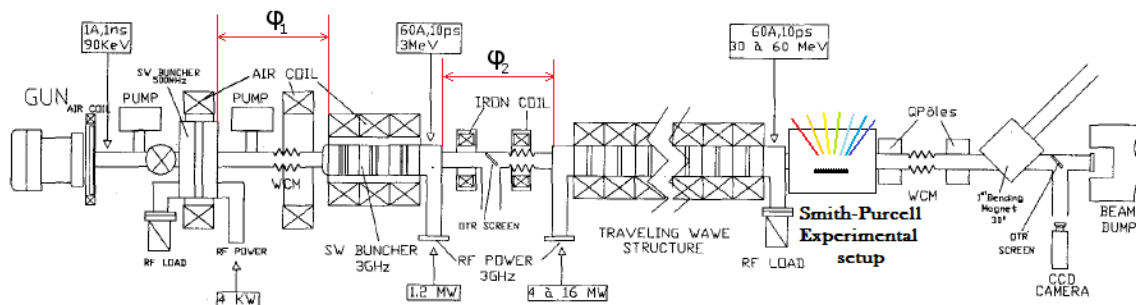

Figure 2: Layout of the CLIO accelerator and position of the experimental setup.

gun, a subharmonic buncher (SHB), a fundamental buncher (FB) and an accelerating cavity (AC). The gun produce bunches about 1.5 ns long at an energy of 90 keV. These bunch are then compressed by the subharmonic buncher to 200 ps or less to make it suitable for further compression with the fundamental buncher. This fundamental buncher further compresses the beam to a few ps and accelerates bunch to several MeV, making the electrons relativistic. The bunches are then further accelerated in the accelerating cavity to the operation energy (typically 10-45 MeV).

For bunch compression the most important parameters are the phases φ_1 (between SHB and FB) and φ_2 (between FB and AC). In our experiment we change bunch length by changing φ_1 and while keeping the beam energy constant at 44.3 MeV.

4 Data processing and analysis

Degree of freedom - grating movement Two stages – proof of SPR and extracting data from it

4.1 Data Acquisition

Data is taken with DAQ board with 250 ksps sampling rate. Python script (read_plot_data.py) Analyze single file with taken data and produce the the array of signals on chosen channels. Noise filtering is implemented inside script. We use simple FFT filtering by turning in zero high frequency component of modulus of FT of the signal. Depth of filtering could be chosen by user. Signal is extracting from filtered data on falling edge of electron signal and computed as difference of signal amplitude at equidistant positions from the edge. This give amplitude on detector when bunch pass grating and with respect to the moment before. Except this electron signal amplitude is acquired as simple min. For this type of the signal we remove constant component with FFT and live other components as they are. After script finish his work, .sig file is generated. In this file, except spectral component and electron signal, we also have some additional information like position of the grating, time and date, etc. After measurements, .sig files are collected and analyzed with matlab.

> **Take into account!!!**
>
> Simple min of electron signal could be source of problems due to inductive character of the line. So measured in this way signal could be over-evaluated.

4.2 Data analysis

As sampling rate is high (250 ksps) and accelerator repetition rate is low (25 Hz), usually in one file we have one signal or no signal at all, but this file anyway was processed. So at the analysis stage we reject data with zero electron intensity by applying the cut in analyzing code. Also we cut events with incorrect measured

amplitude by cutting single high-amplitude events on 12 channel, as this channel didn't see signal and only noise. All the data normalized by electron signal intensity.

4.2.1 Smith-Purcell theory prediction

According to Smith-Purcell theory, we expect to see exponential decay of the signal as function of beam-grating separation

Figure 3

4.2.2 Experimental results

We made wide scan of amplitudes for different beam-grating separation. But instead of clear exponent we see in figure 4 complicate curve. Result is reproducible for two different buncher phases. For different angles shape of the curve is different, but all of them have exponential increase close to beam (or linear in log scale). So further measurements will be done in this narrow region near the beam.

Its clear seen from figures 4, that except SP signal in total signal present also background, which have non random behaviour, as we could also see from figures 5. With approaching to the beam, we saw increase of the signal – probable SP radiation. At region far from the beam, we see some pattern, nature of which should be investiagated.

In log scale we could see in figure 6 two signal components: SPR signal (we suppose) and background.

As we could see, we could measure signal only in small region near beam, which in real life could impact on beam. So background rejection technique's should be applied (THz mesh or WAP filters).

We divide signal in region of break by two subregions: background (fitted by grey lines) and signal (color lines). We assume that in this narrow region background is constant, so we fit data from -Inf (approx 20 mm) to intercept of two "lines" (background and signal). This give us background level. Then we choose data points, which are higher than this level and fit them be exponent. This method allow us get better fit, when signal level is low.

In result we have three coefficints: background, amplitude of the signal and decay wavelength.

During first part of our experiment we change bucher phase ϕ_B of the accelerator. Of course this also change the the electron beam intensity as shown on figure 7a. Each time signal was normalized by this value.

> **Take into account!!!**
>
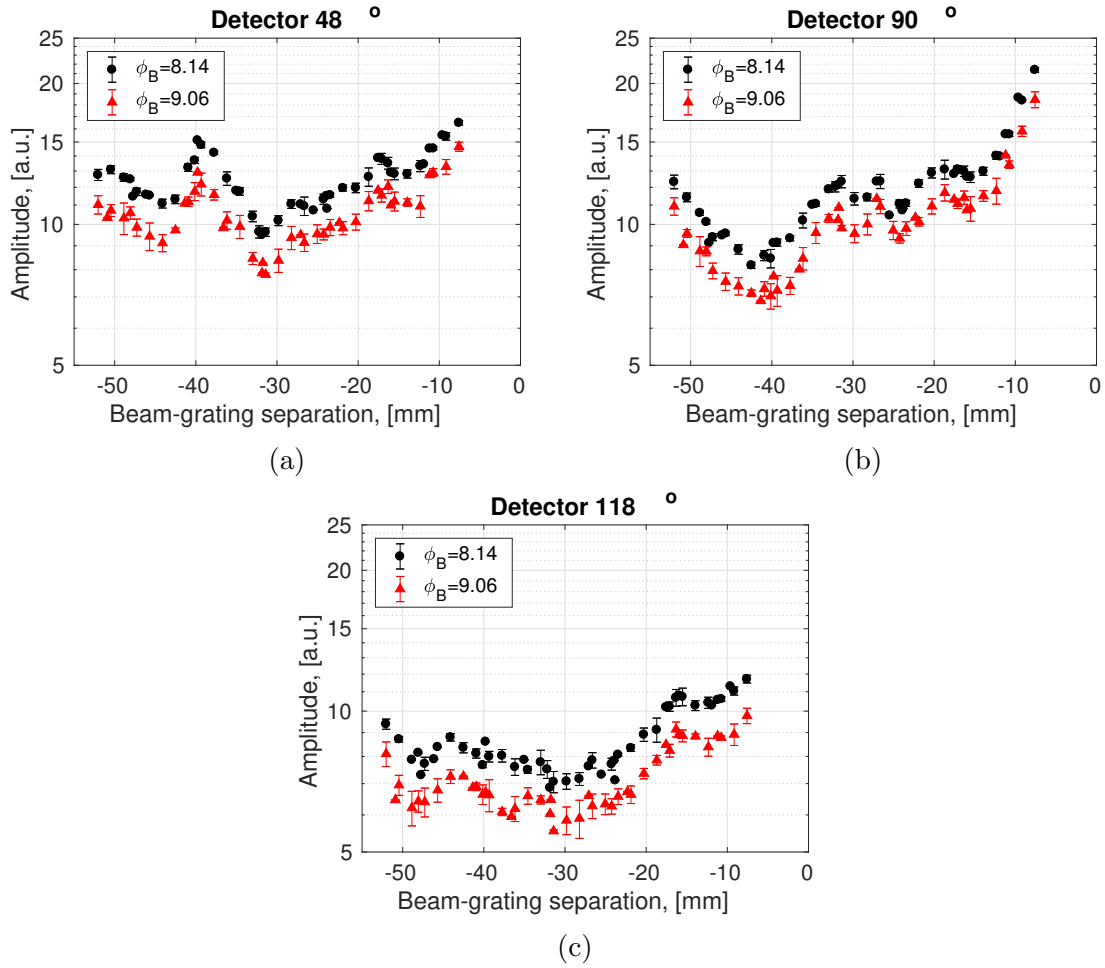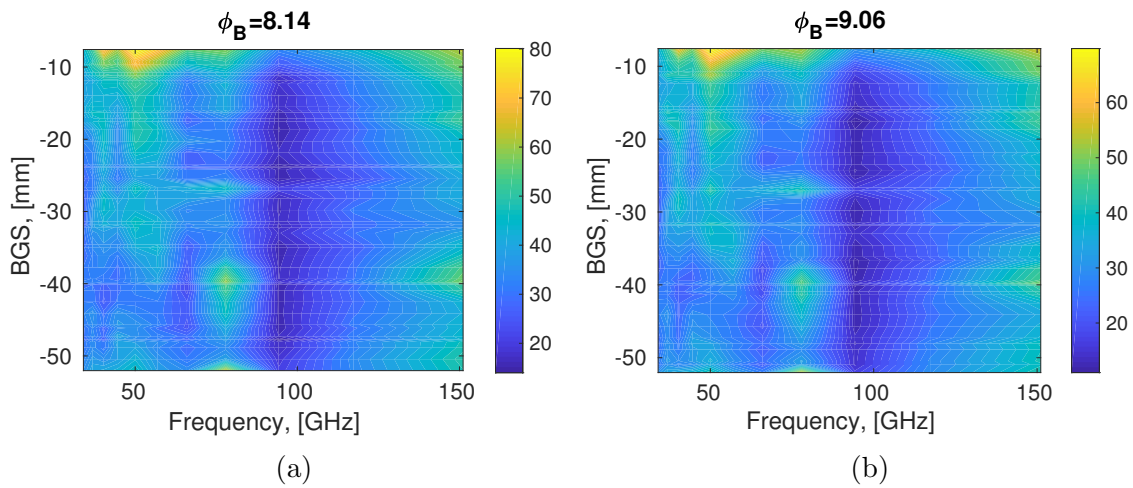> Energy spread should be taken into account in gfw calculation

Figure 4

Figure 5

Figure 6

(a)

(b)
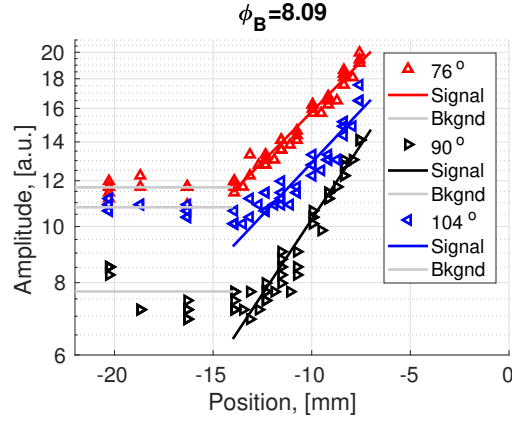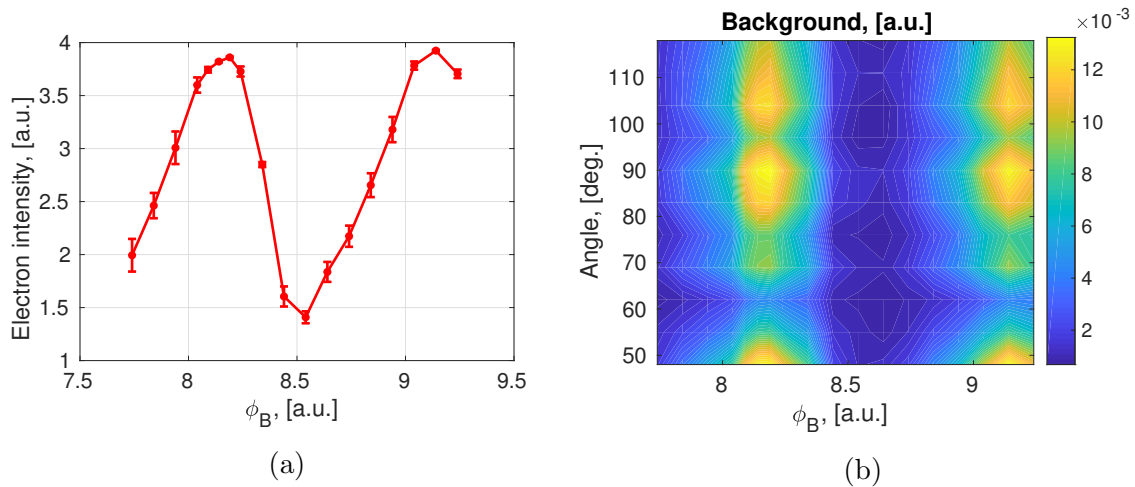
Figure 7

As we see on figure 7b value of background is also changing as function of phase. Reader should take into account, that signal, which is used to fit the background was normalized by electron signal.

> **Take into account!!!**
>
> Nature of background and the methods of background rejection require further investigation

Lets look in detail in this data.

As was mentioned above, decay length of SP signal if angle-dependent and could be used as indicator of SPR from side and theck of alignment from other side. We fing that with "good bunch", decay wavelength is stable and phase independent, as it should be. When the signal is low, we have bad fit and distorted result. This guess could be proofed by R^2 map of goodness of fit (see fig. 9). Its could be alos caused by change of gamma factor. From other side, this could indicate on other effect, which

is measured by our system.
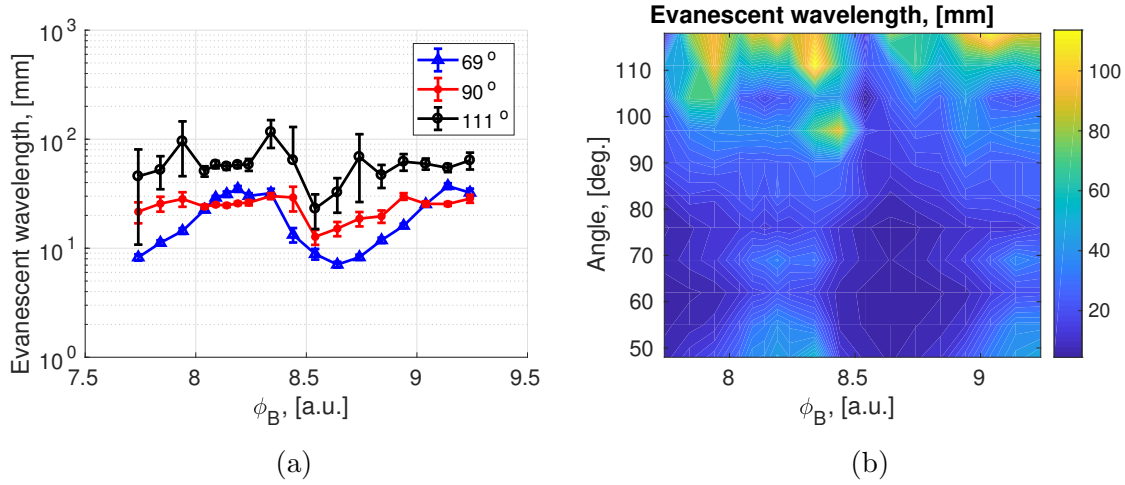
Figure 8
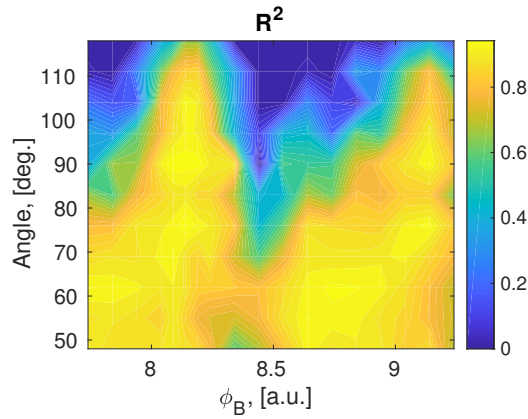
Figure 9

We take weighted mean and compare evanescent wavelength with predicted by the theory of SPR. From figure 10 we see total tilt of 2 degrees. Particularly it could be caused by misalignment of the optical system. Because of long measured wavelengthes, focal spot is also big, so input aperture of the OAP mirror is bigger.

> **Take into account!!!**
>
> Calculate this correction. Also decay in quartz window (+ reflection), and air

Decay length at 48° is bigger that predicted, so in this signal component could impact also other effect.
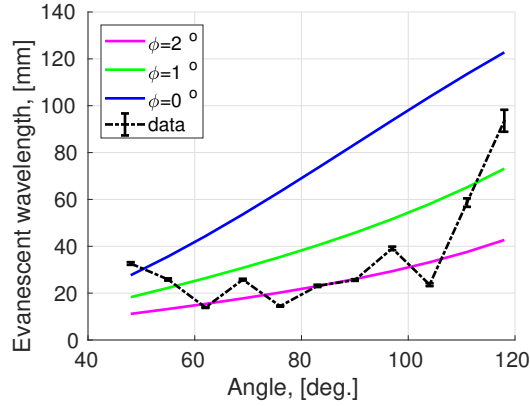
Figure 10

Take into account!!!

Behaviour of evanescent wavelength require further experimental checks and advanced correction (acceptance angle ...) in theory!

Amplitude plots on figure 11 present spectrum at 0 beam-grating separation. We see that is changing with buncher phase. Angular components changing independently, contrary to background change, so we could assume, that it was caused by coherent phenomenas and we could hope that we could see also bunch shape change. Detail investigation of spectrum and Form Factor at different beam-grating separation will be done later.

(a)   (b)
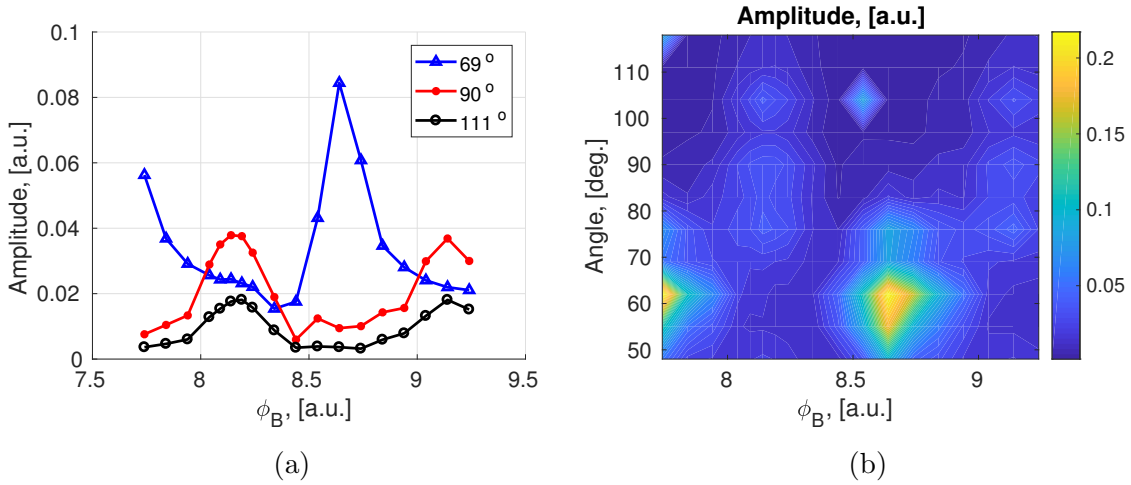
Figure 11

5 Spectrum analysis

Using fitting results, we could more precisely reconstruct spectrum and reject background. Using GFW code and experimental setup correction, we could calculate single electron yield and predicted spectrum for certain bunch length and shape. In figure 12a is shown measured spectrum for buncher phase equal $\phi_B = 8.14$ and three spectrums for gaussian beam and different bunch duration. By width the most situable is 5ps gaussian bunch. Difference from measured one could be explained by a bit more complex bunch structure that simpe gaussian. From other side, we measure train of pulses, so it could be, that microbunches in train have different width. Spectrum change, as function of phase is shown in figure 12b. BGS for this two spectrums is 10 mm
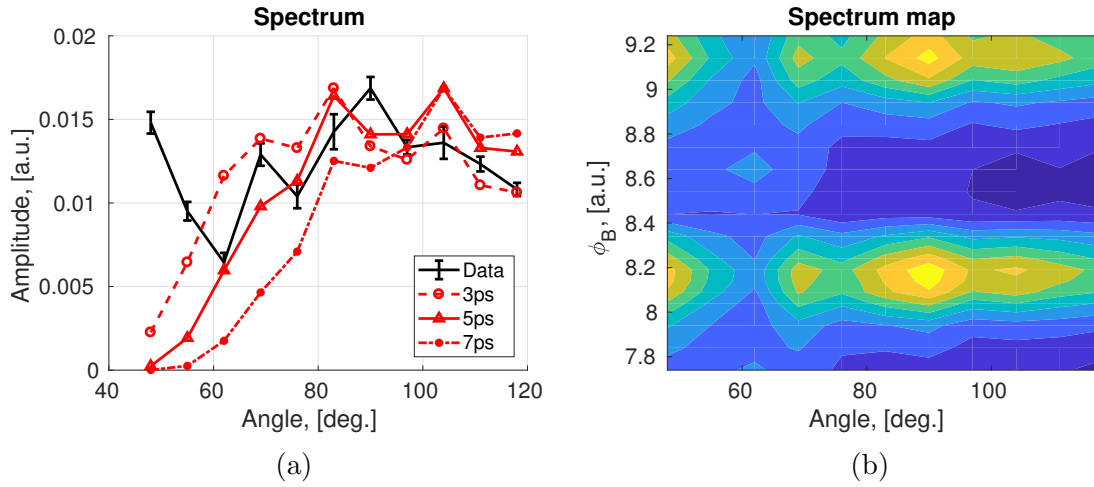
Figure 12

5.1 Form Factor

We expect to see same Form factor as function of BGS, but from figures 13 we see rapidly changing components as function of BGS. We suppose that it is parasite radiation.

> **Take into account!!!**
>
> Take into account in gfw code different angle of observation (ϕ). Take into account correction on aberration (ellips+circle)

Form factor for phase for buncher phase equal $\phi_B = 8.14$ is shown on figure 14a. Its vary in amplitude, but save its shape ap function of BGS. Change of amplitude was caused by disagreement of evanescent wave in computation code and experimental data.

9

Form Factor (BGS=5 mm)

Form Factor (BGS=10 mm)

(a)

(b)

Form Factor (BGS=15 mm)

(c)

Figure 13

FormFactor

Form Factor (BGS=10 mm)

(a)

(b)
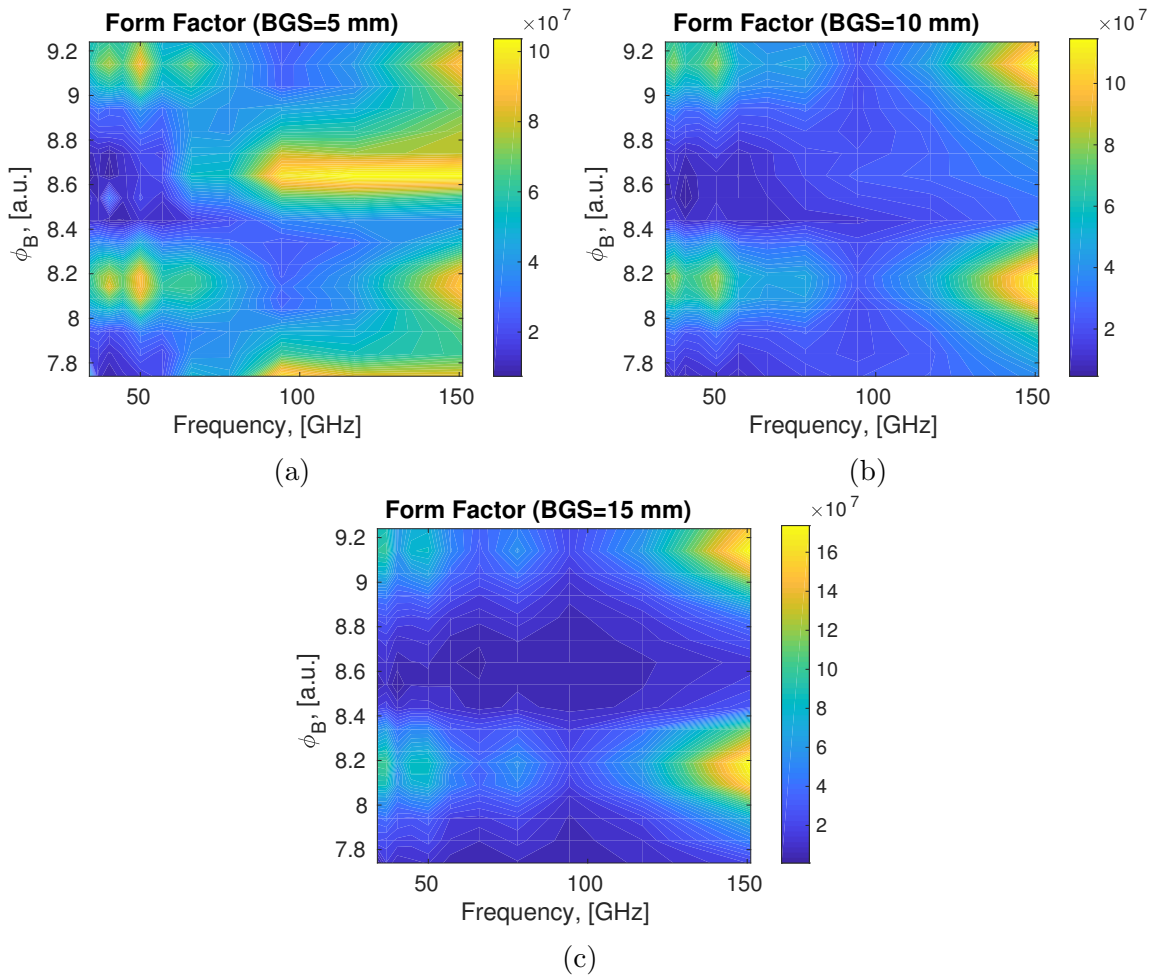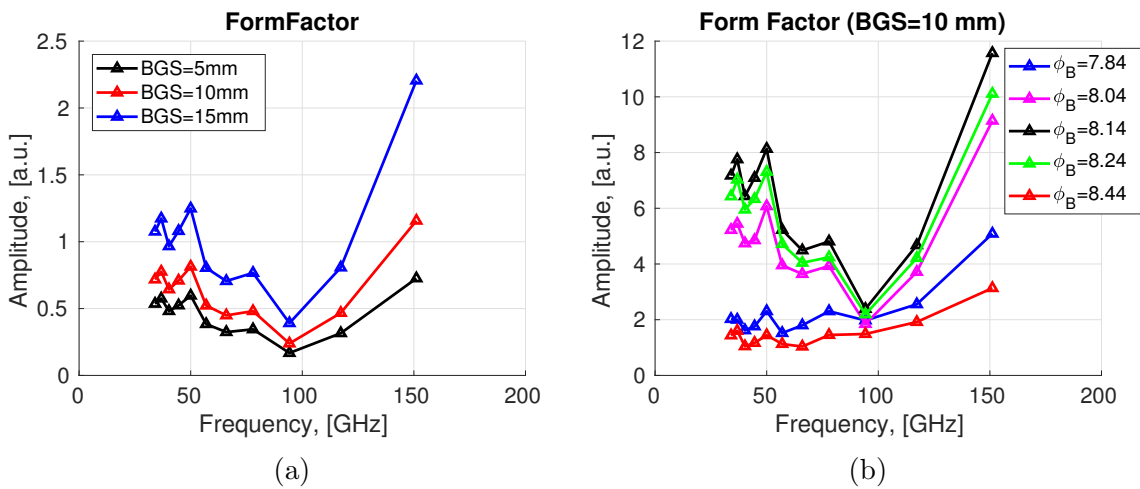
Figure 14

6   Bunch profile reconstruction

We apply spectrum recovery procedure as was mention in [?]. We use most optimized bunch form-factror ($\phi_B = 8.14$) for normalization of the the form-factors of others bunches. In our reconstruction we didnt take into account first two points in spectrum.

> **Take into account!!!**
>
> A lot depend on Spectrum normalization. Now its completely arbitrary choise.

The result of spectrum recovery for several bunch phases is presented on figure 15. Next step is profile recovery. At this point we use Hilbert method of phase recovery,
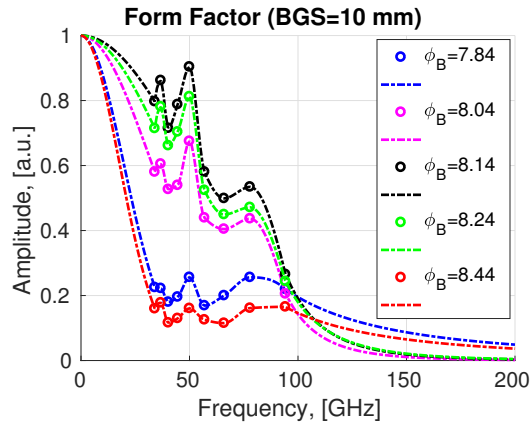
Figure 15

as it gives the best result [?]. After we made inverse Fourier transform. Result of reconstruction is presented on figure 16.

(a)

(b)
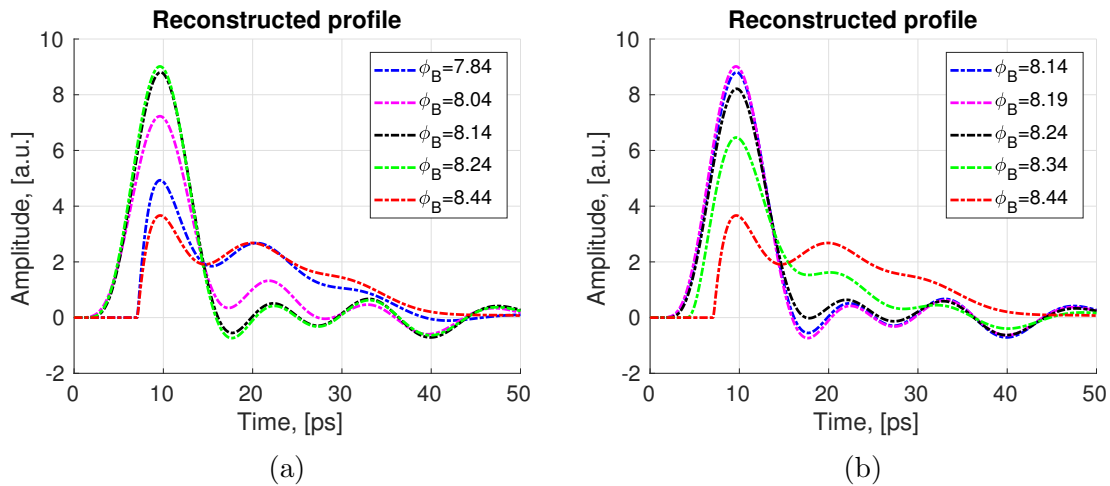
Figure 16

Change of bunch width at 10%, 50% and 90% of maximum is presented on figure 17a. For phase $\phi_B = 8.14$, we have: FW0.1M=2.7ps, FWHM=6.8ps, FW0.9M=11.1ps.
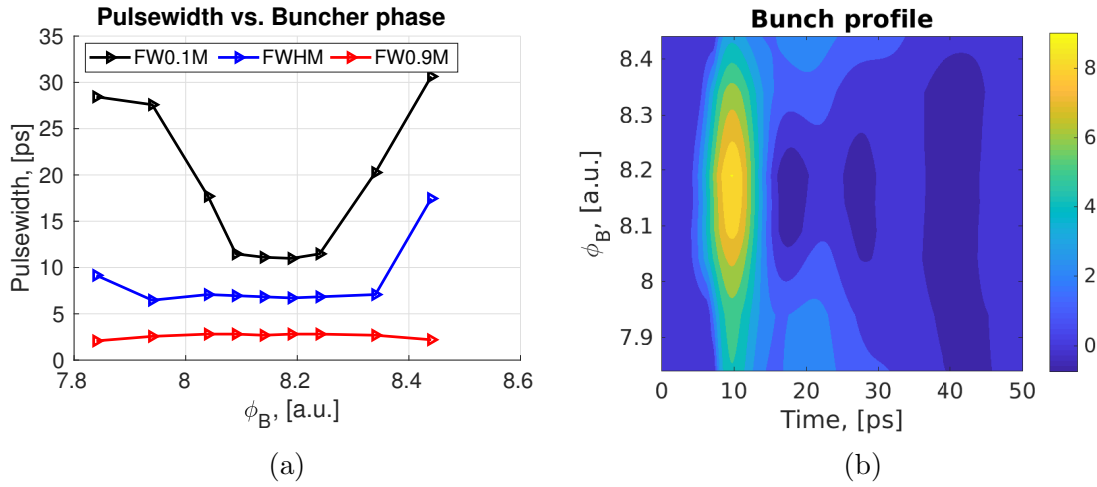
Figure 17

To check the correctness of the procedure we calculate spectrum with this achieved profile and compare it with measured (see figure 18a). The difference shwo that in spectrum we have exponential with angle component, which is background. Nature of this component is under investigation.

Also, to estimate error of profile reconstruction, we introduce noise in spectrum in calculated error bounds and reconstruct profile (set of 100 profiles). We get that $FWHM = 6.8 \pm 0.3ps$ within 3 sigma change of the spectrum components.
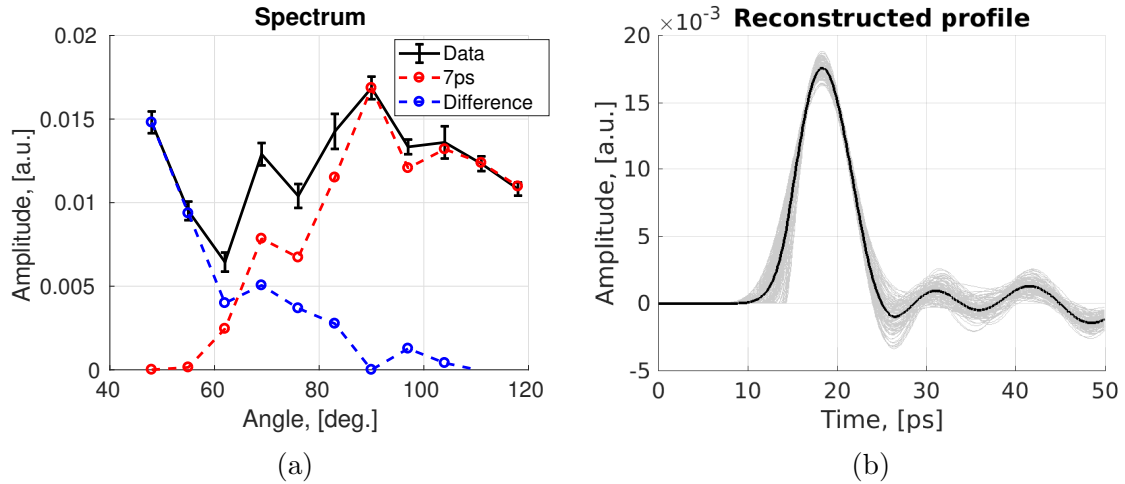
Figure 18

7   Buncher power

Same study was done for spectrum's as function of buncher power. We made same procedure of data extraction, but get other behaviour of coefficient change (see 19). Coefficient stay constant until reaching the bunch power equal 1.2. Peak of evanescent wavelengthes was caused by bad fitting of data curve (as result of noisy data).
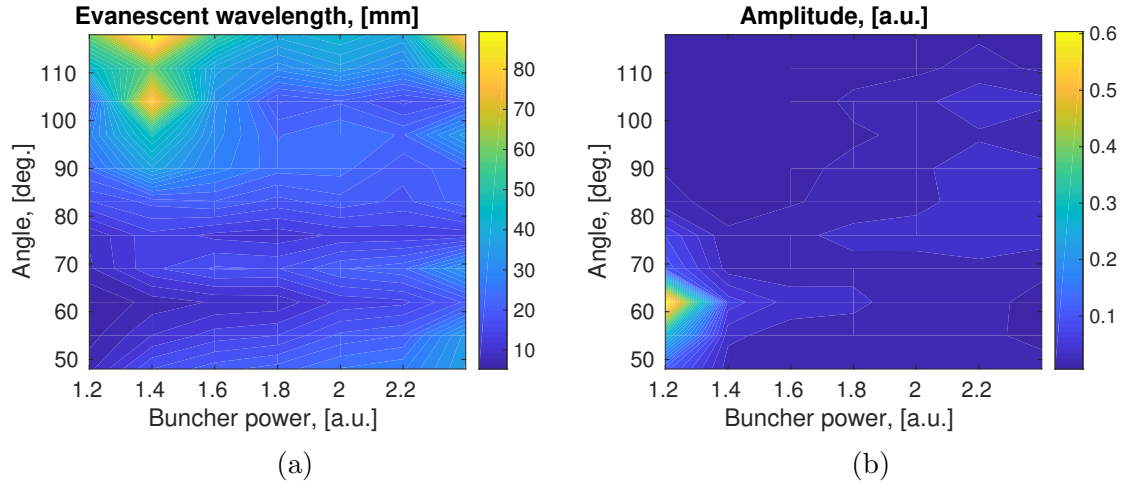
Figure 19

In particular case (see 20) we see small increase in amplitude and alsomost constant change in evanescent wavelength. As "theoretical" we suppose increase in bunch energy from 38.2 MeV for 1.2 [a.u.] of buncher power to 44.2 MeV at maximum buncher power. In this range of energies, evanescent wavelength almost not change (small decrease), as shown on figure 20a by solid line. In general evanescent wave-
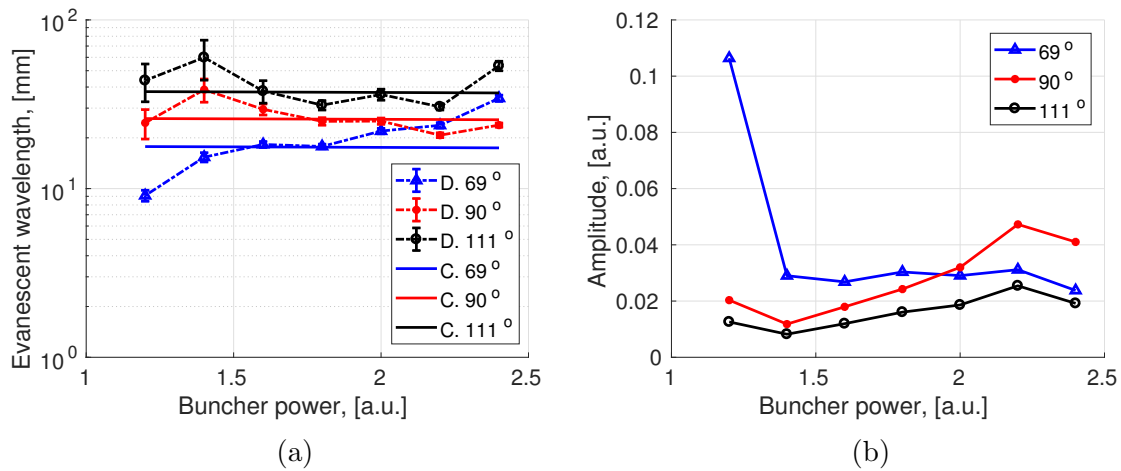
Figure 20

length is in the previous trend (see fig. 21)
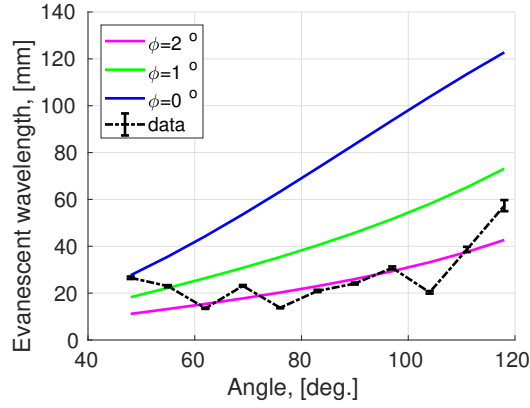
Figure 21

Spectrum change as function of buncher power is presented on figure 22a and 22b. With low power of buncher, Its impossible to form good bunch for futher acceleration.
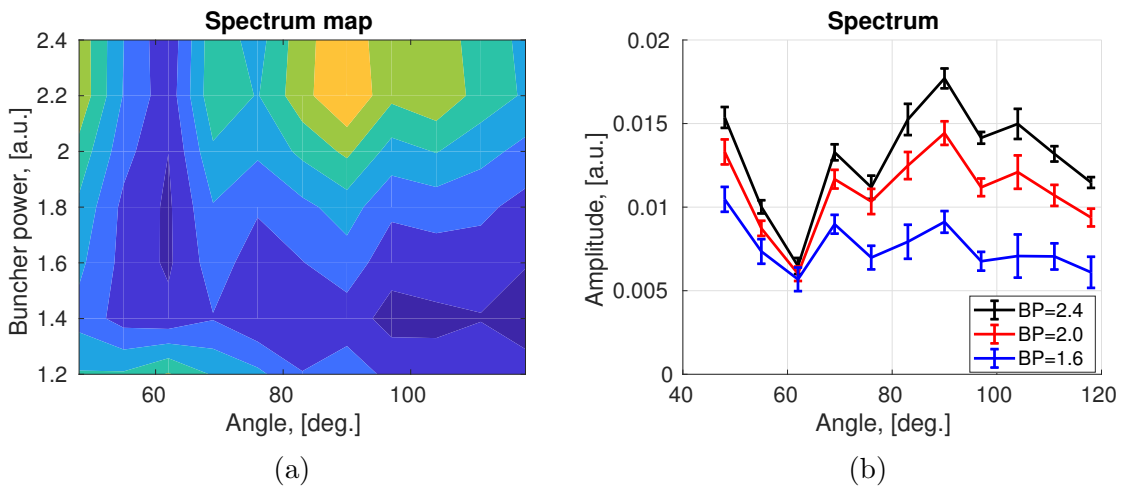
Figure 22

On figure 23a presented interpolated and extrapolated Form factor. FWHM and FW0.1M not really depend from buncher power, but FW0.9M increase almost twice with decrease of buncher power. That indicate on bad compression.
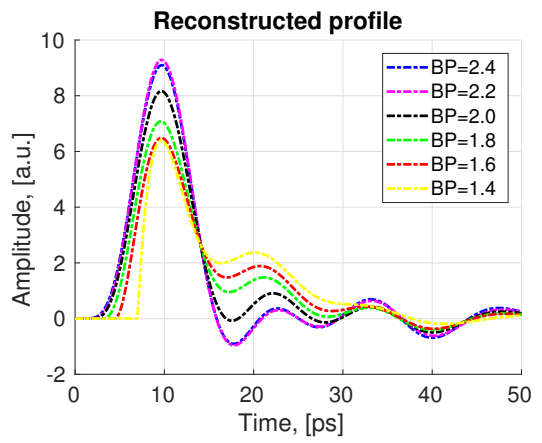
Profile evolution is presented on figure 24
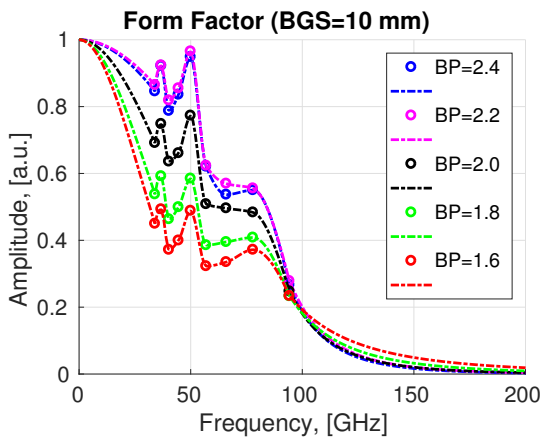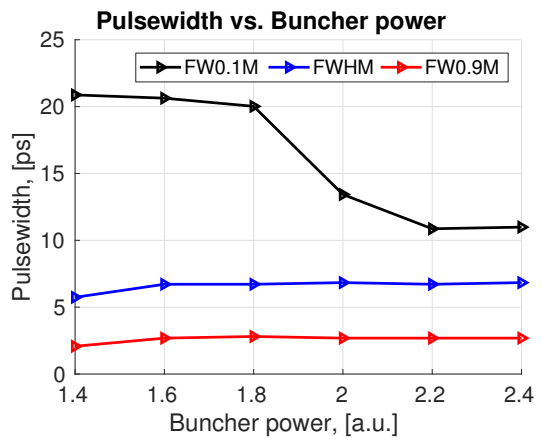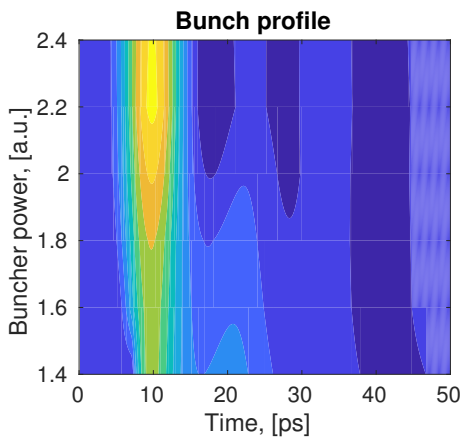
Figure 23

Figure 24

8 Section phase

Using same method, we obtain follow map for fitting coefficients (see fig. 25a and fig. 25b)

(a)   (b)

Figure 25

(a)   (b)
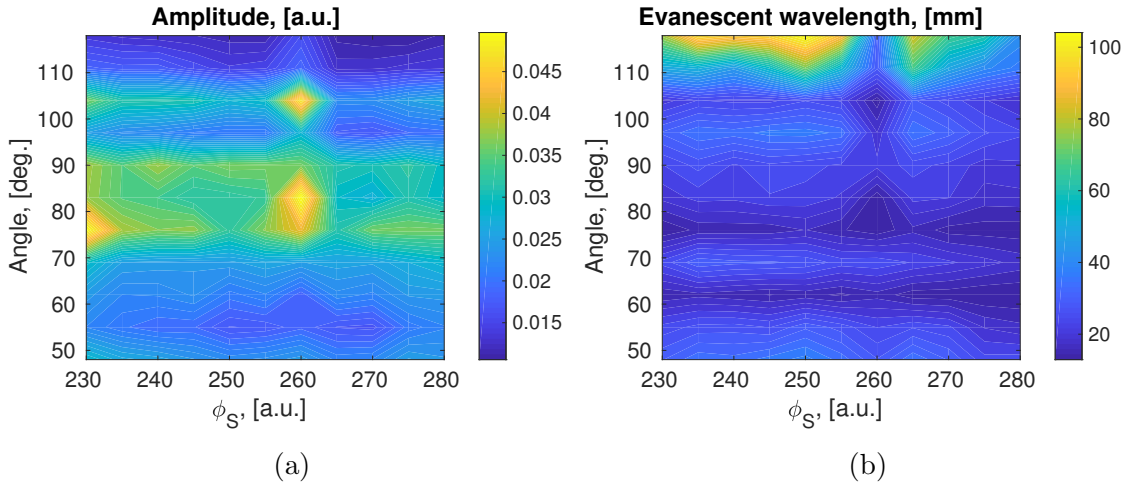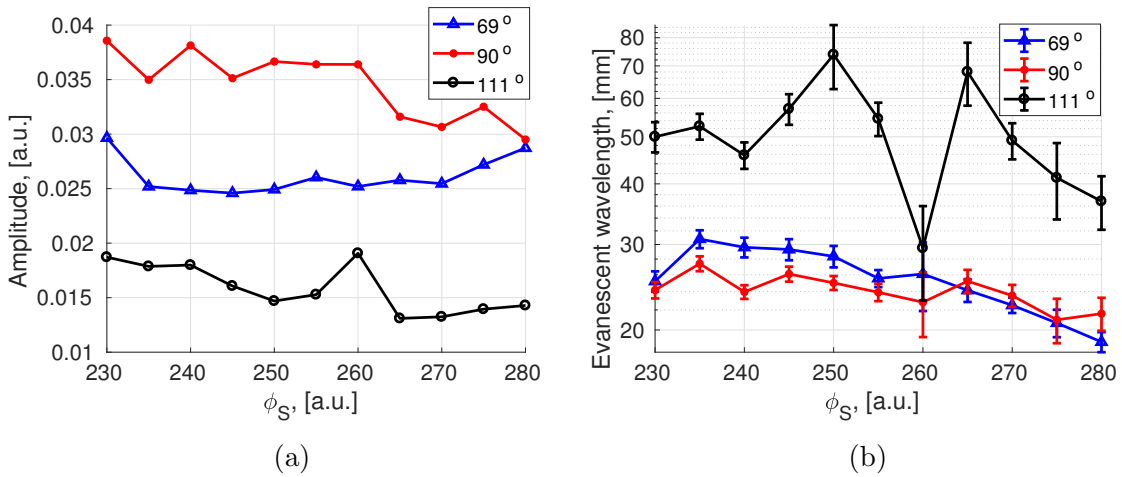
Figure 26

> **Take it into account!!!**
>
> SEY for 44.2 MeV

In this calculation was negleged change of SEY, but even with this assumption we see that profile didnt change a lot, as we espect. Second conclusion:
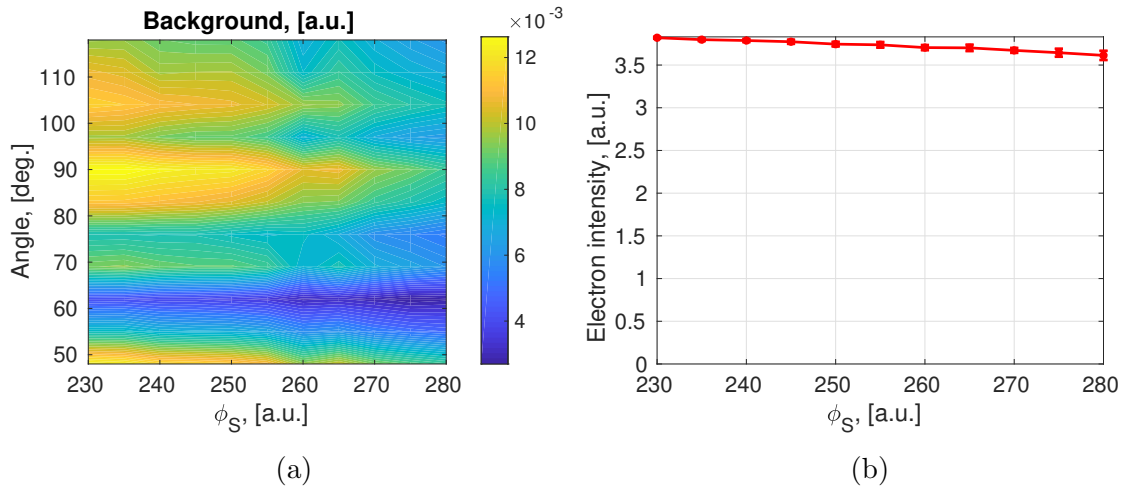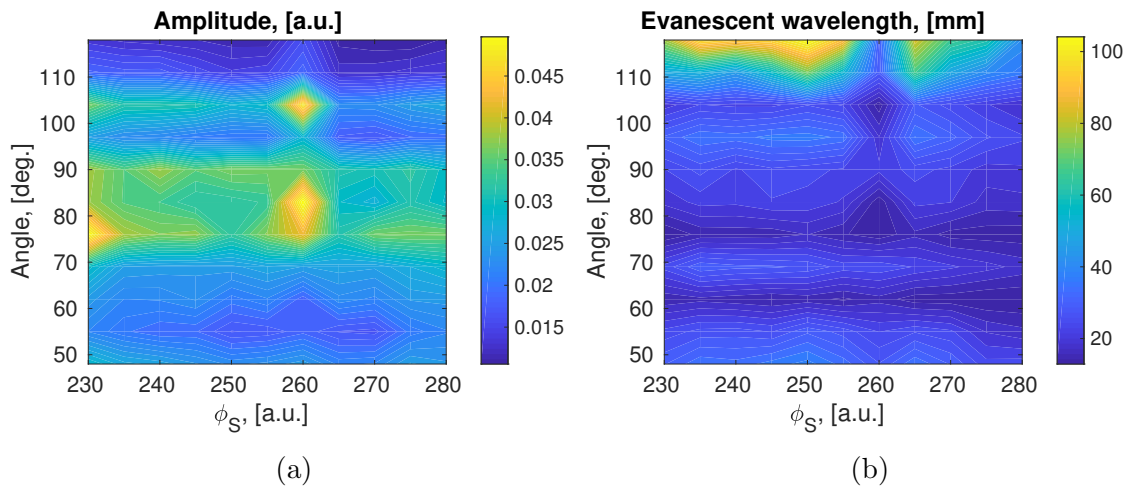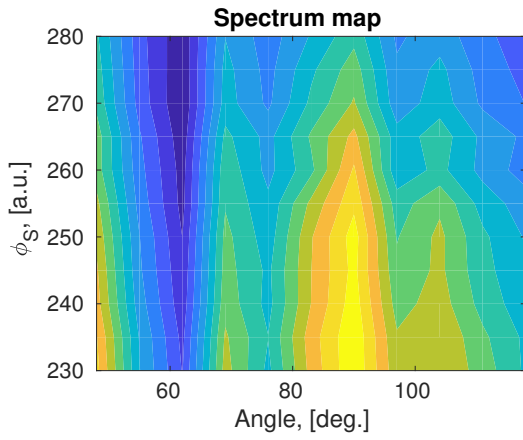
Figure 27

Figure 28

Make this study!!!

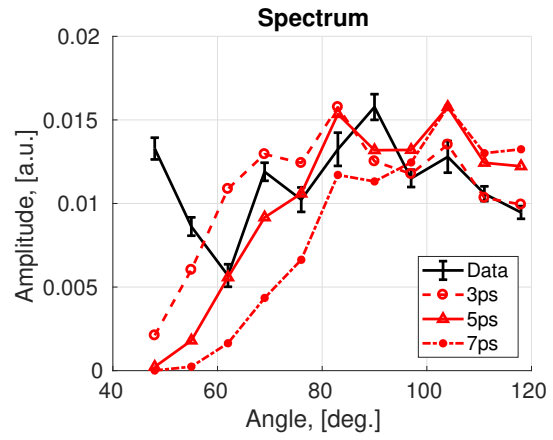Is current setup is sufficient to study change of spectrum as function of bunch energy.
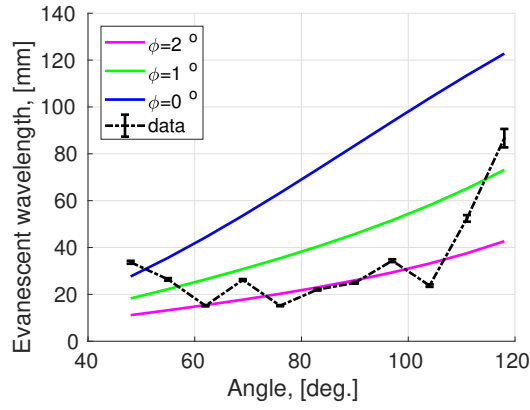
Figure 29

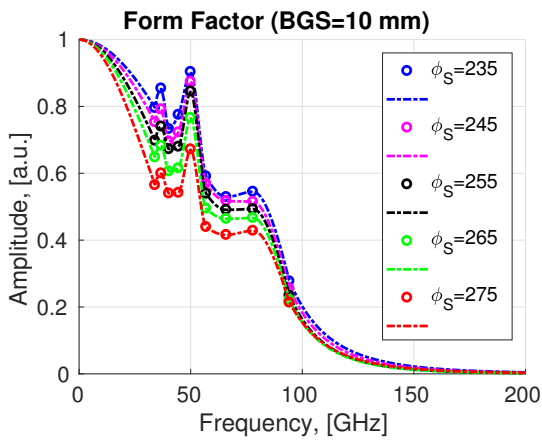

(a)   (b)
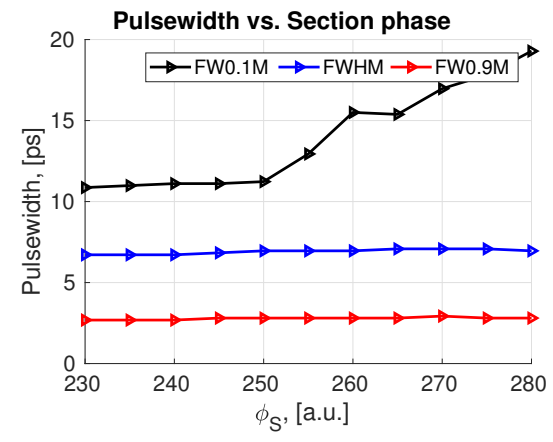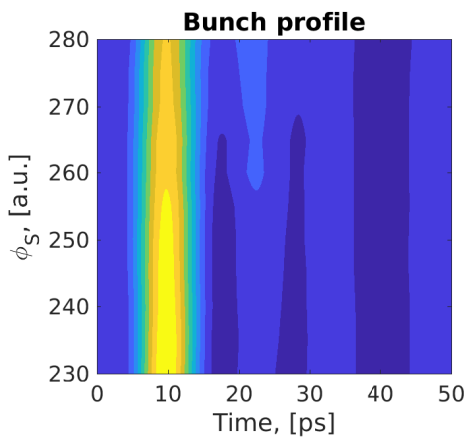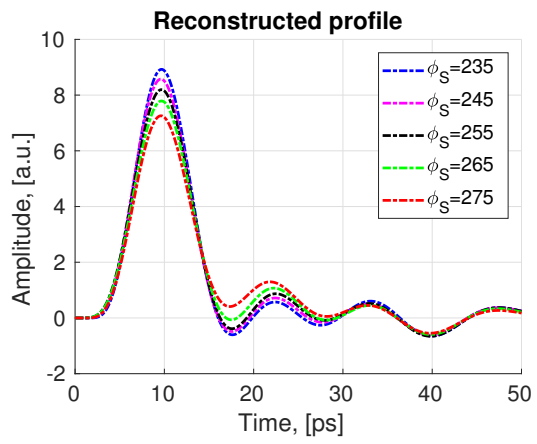
Figure 30

(a)   (b)

Figure 31

18

Figure 32

19

Primary comparison with ASTRA simulation
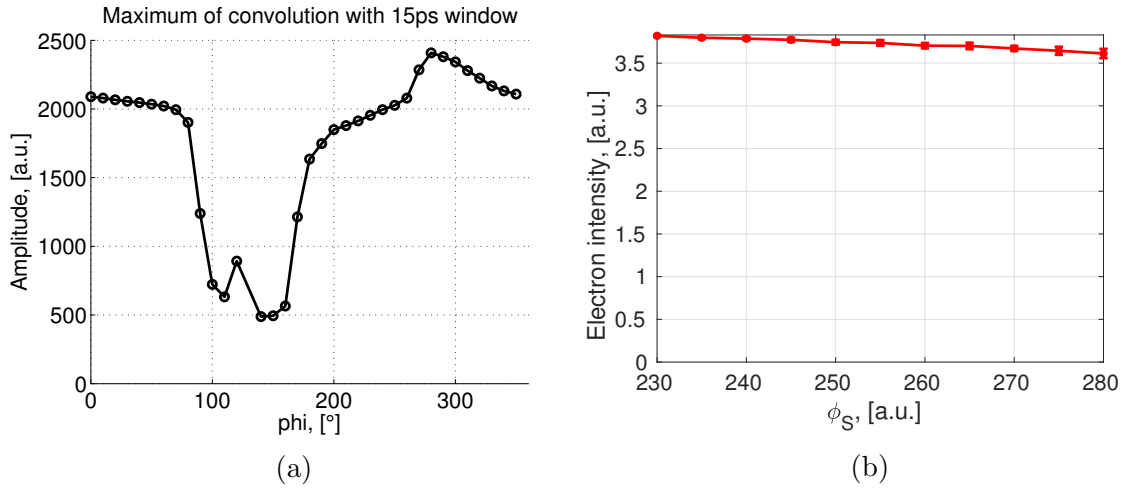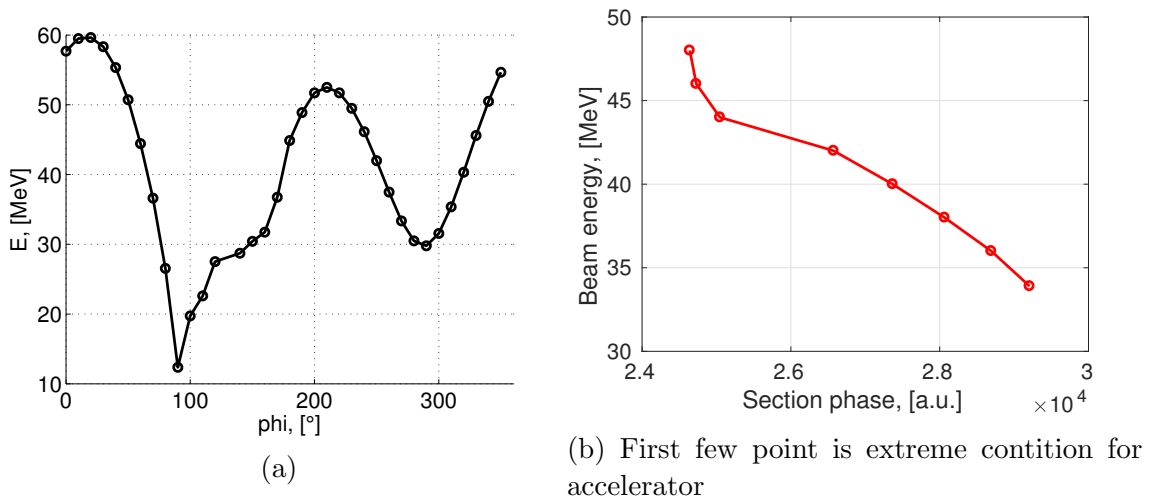

(a)

(b)

Figure 33

(a)

(b) First few point is extreme contition for accelerator

Figure 34

At this point we could conclude, that we are at the beginning of phase diapason, because:

- Electron intencity not depend a lot from section phase

- We have similar behaviour of beam energy from section phase

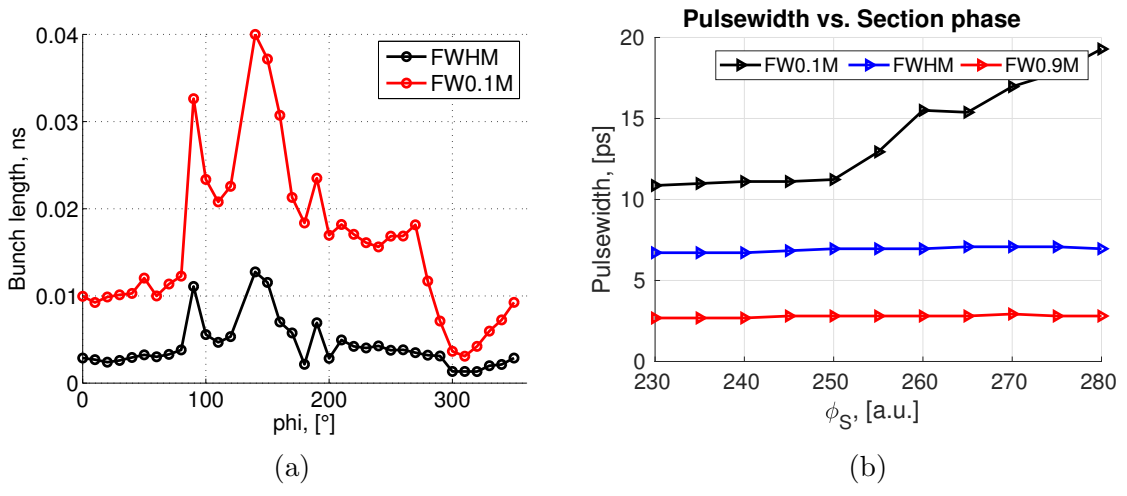- FWHM and FW0.1M also have similar behaviour in this region

(a)

(b)

Figure 35

Make this study!!!

Should be developed advanced model of CLIO accelerator. Results of SPR measurement should be compared with ASTRA model!

9 Conclusion

"I always thought something was fundamentally wrong with the universe" [**?**]

10 Appendix

10.1 Position calibration

One step of motor equal 7.94 nm. For current calibration we use motor steps as reference.

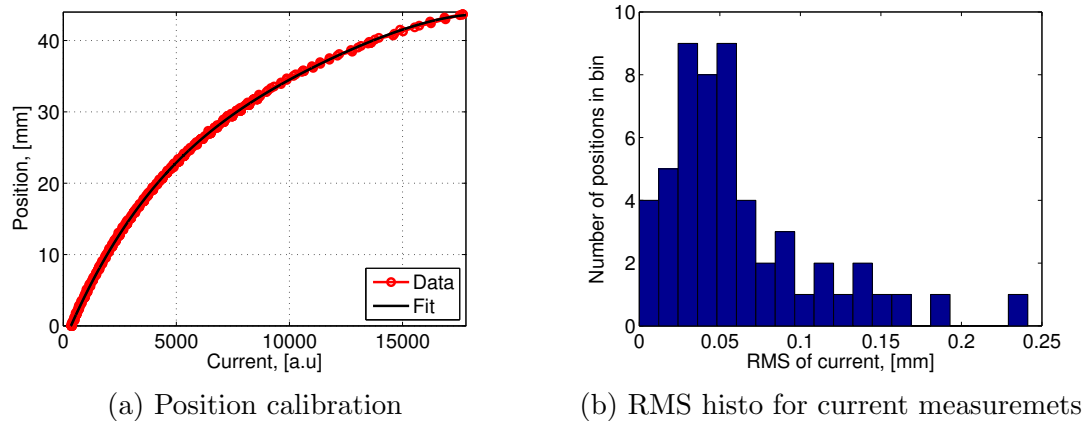(a) Position calibration (b) RMS histo for current measuremets

Figure 36: Position calibration

With polynomial fit we get:

$$f(x) = -8.374e - 11 * x^4 + 4.053e - 06 * x^3 + -0.08082 * x^2 + 952.6 * x - 3.141e + 05$$

As current measurements are variable in time for same position. By taking fit of this data with gaussian, we find peak at the **0.04 mm**, which define precision of position determination with potentiometer.

10.2 Correction of defocusing

Turned by defined angle, mirror saw bigger grating surface (ellipse). If grating is small, ellips could be bigger than grating. Cross-section of ellipse and rectangular define this correction. Script Grating_correction.m

10.3 Mirror acceptance

Cross-section of two circles (detector and focus point of abbe diffraction limit).
    Focus spot is circle with radius defined by Abbe difraction limit. Detector diameter is fixed and equal 2 mm and supposed to be exactly in focus of 25mm with 50.8 focus length OAP mirror.
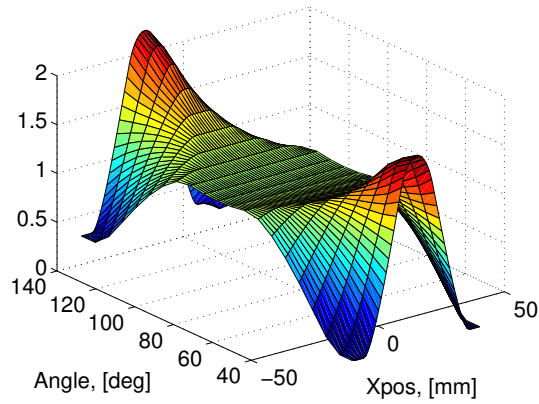
Figure 37: Correction on defocusing for 25 mm spherical mirror and 20x40 mm grating size as function as grating position

Also was taken into account, that frequency of SPR depent from observation angle, so at different angle we have different spot size. Script OverlapCorrections.m

10.4 Beam size

This experiment was done by cutting with 3 mm grating beam and measuring electron intensity. Grating tooth height should be taken into account! Script Beam_size.m
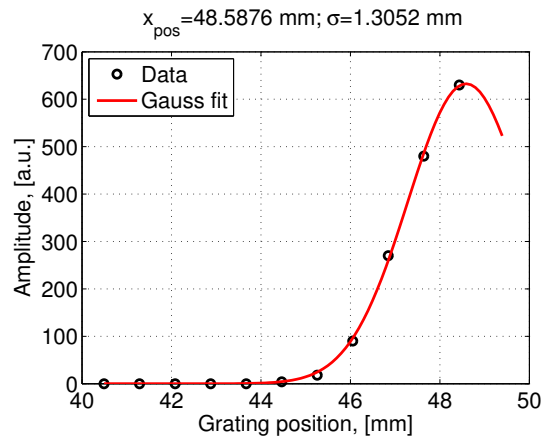

Figure 38: Transverse beam size at CLIO

10.5 Section phase/energy
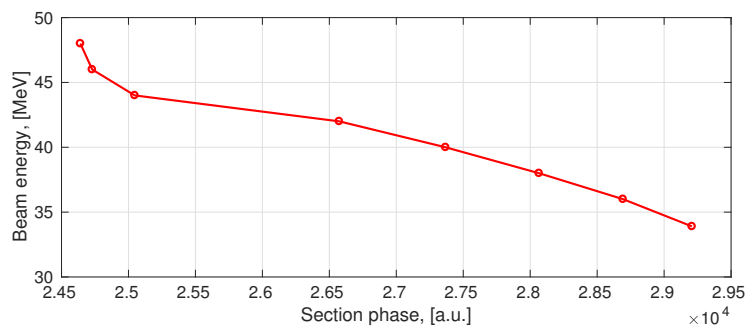
Calibration of Section phase vs. Energy. Script PhaseEnergy.m

Figure 39: Section phase vs. beam energy